Author/s:
Li, Y;Ryu, D;Western, AW;Wang, QJ

Title:
Assimilation of stream discharge for flood forecasting: Updating a semidistributed model with an integrated data assimilation scheme

Date:
2015-05-01

Citation:
Li, Y., Ryu, D., Western, A. W. & Wang, Q. J. (2015). Assimilation of stream discharge for flood forecasting: Updating a semidistributed model with an integrated data assimilation scheme. Water Resources Research, 51 (5), pp.3238-3258. https://doi.org/10.1002/2014WR016667.

Persistent Link:
https://hdl.handle.net/11343/297395

AGU PUBLICATIONS

Water Resources Research

RESEARCH ARTICLE
10.1002/2014WR016667

Key Points:
- A semidistributed model leads to better forecasts than a lumped model
- The superiority of the semidistributed model becomes less significant after DA
- Assimilating discharge at the catchment outlet gauge showed a limited or no skill to improve streamflow forecasts at 'ungauged' internal locations.

Correspondence to:
D. Ryu,
dryu@unimelb.edu.au

Citation:
Li, Y., D. Ryu, A. W. Western, and Q. J. Wang (2015), Assimilation of stream discharge for flood forecasting: Updating a semidistributed model with an integrated data assimilation scheme, *Water Resour. Res.*, *51*, 3238–3258, doi:10.1002/2014WR016667.

Received 12 NOV 2014
Accepted 4 APR 2015
Accepted article online 8 APR 2015
Published online 8 MAY 2015

Assimilation of stream discharge for flood forecasting: Updating a semidistributed model with an integrated data assimilation scheme

Yuan Li[1,2,3], Dongryeol Ryu[1], Andrew W. Western[1], and Q. J. Wang[2]

[1]Department of Infrastructure Engineering, University of Melbourne, Parkville, VIC, Australia, [2]CSIRO Land and Water Flagship, Highett, VIC, Australia, [3]Now at Department of Civil Engineering, Monash University, Clayton, VIC, Australia

Abstract Real-time discharge observations can be assimilated into flood models to improve forecast accuracy; however, the presence of time lags in the routing process and a lack of methods to quantitatively represent different sources of uncertainties challenge the implementation of data assimilation techniques for operational flood forecasting. To address these issues, an integrated error parameter estimation and lag-aware data assimilation (IEELA) scheme was recently developed for a lumped model. The scheme combines an ensemble-based maximum a posteriori (MAP) error estimation approach with a lag-aware ensemble Kalman smoother (EnKS). In this study, the IEELA scheme is extended to a semidistributed model to provide for more general application in flood forecasting by including spatial and temporal correlations in model uncertainties between subcatchments. The result reveals that using a semidistributed model leads to more accurate forecasts than a lumped model in an open-loop scenario. The IEELA scheme improves the forecast accuracy significantly in both lumped and semidistributed models, and the superiority of the semidistributed model remains in the data assimilation scenario. However, the improvements resulting from IEELA are confined to the outlet of the catchment where the discharge observations are assimilated. Forecasts at "ungauged" internal locations are not improved, and in some instances, even become less accurate.

1. Introduction

Accurate and timely forecasting of potential river floods, one of the most destructive natural disasters, is a necessity for providing warnings and initiating emergency response. However, the forecasts are inherently uncertain due to errors in model initial condition (state variables), input forcing (numerical weather prediction outputs), model parameters, and model structure. Data assimilation (DA) provides a way to integrate real-time observed information into forecasting models to improve the forecasts by reducing errors in initial conditions and/or parameters. With the development of novel statistical methods and observational techniques, DA is becoming an important component of hydrologic forecasting [*DeChant and Moradkhani*, 2012; *Hendricks Franssen and Kinzelbach*, 2008; *Lee et al.*, 2012; *Li et al.*, 2013; *Liu et al.*, 2012; *Moradkhani et al.*, 2012; *Nie et al.*, 2011; *Ricci et al.*, 2011; *Thirel et al.*, 2010a; *Vrugt et al.*, 2013]. Although advanced remote sensing techniques provide an opportunity to improve hydrologic simulation [*Alvarez-Garreton et al.*, 2014; *Crow and Ryu*, 2009; *DeChant and Moradkhani*, 2011; *Massari et al.*, 2014; *Wanders et al.*, 2014], gauged discharge DA is a more effective way to improve short-term forecasts and thus it is still preferred for operational streamflow forecasting purposes [*Komma et al.*, 2008; *Lee et al.*, 2011, 2012; *Li et al.*, 2014; *Liu et al.*, 2012; *McMillan et al.*, 2013; *Rakovec et al.*, 2012; *Seo et al.*, 2009; *Vrugt et al.*, 2006].

Despite the recent advancements in discharge DA for hydrologic modeling, there still remains various challenges [*Liu et al.*, 2012]. One important challenge is the natural time lags related to the flow routing processes. It has been identified that these time lags do not cause an issue for filtering methods when the model is formulated as a first-order Markov model (e.g., storage routing models); however, when a Markov model with an order higher than one is used (e.g., unit hydrographs), conventional filtering methods become a suboptimal choice [*Li et al.*, 2011, 2013; *Weerts and El Serafy*, 2006]. Various methods have been introduced to address the time lag issue, including variational DA [*Lee et al.*, 2011, 2012; *Seo et al.*, 2009], the lagged particle filter [*Noh et al.*, 2011], the retrospective ensemble Kalman filter (EnKF) [*Pauwels and De Lannoy*, 2009], the recursive EnKF [*McMillan et al.*, 2013], and the EnKS [*Li et al.*, 2013, 2014]. The retrospective

EnKF, recursive EnKF, and EnKS are three variants of the EnKF. The EnKS can pass the observation information to the antecedent model states as effectively as the other two and it is found to improve the discharge more effectively than the retrospective EnKF by avoiding the recalculation of the updated states from the beginning of the time window [*Pauwels and De Lannoy*, 2009], and to be much more efficient than the recursive EnKF by avoiding the "iterative" update-prediction process [*McMillan et al*., 2013]. Only the rerun of the routing modules—the observation operator—is needed for the EnKS [*Li et al*., 2013].

Another major challenge in DA is error quantification. Efficacy of stochastic DA, to a large extent, is determined by the realistic representation of errors in the model and the observations. Despite this, probabilistic representation of model predictions and observations for stochastic DA is often generated using arbitrary specifications of the error models and parameters [*Liu et al*., 2012]. Nevertheless, more objective methods exist. One such method is automatically tuning error parameters in the online cycling of a filtering system using adaptive filtering approaches [*Crow and Reichle*, 2008; *Crow and van den Berg*, 2010; *Crow and Yilmaz*, 2014; *Reichle et al*., 2008] or the variable variance multiplier approach [*Leisenring and Moradkhani*, 2012; *Moradkhani et al*., 2012]. Another method is informally/formally estimating uncertainties through likelihood-based or Bayesian analysis methods, which disaggregate the difference between the observation and model prediction into different sources of uncertainties. Examples include the Bayesian total error analysis (BATEA) [*Kavetski et al*., 2006; *Renard et al*., 2011], integrated Bayesian uncertainty estimator (IBUNE) [*Ajami et al*., 2007], and the differential evolution adaptive metropolis (DREAM) algorithm [*Vrugt et al*., 2008]. These likelihood-based or Bayesian analysis tools have yet to be more widely used to inform error parameters for hydrologic DA. Notable exceptions are the two recently developed methods that attempt to address this issue: the integrated uncertainty and ensemble-based DA (ICEA) system [*He et al*., 2012] and the integrated error parameter estimation and lag-aware DA (IEELA) scheme [*Li et al*., 2014].

ICEA adopts DREAM to quantify parameter uncertainties and uses the EnKF to improve the discharge forecasts. It was used to assimilate snow water equivalent data and found to outperform the stand-alone EnKF in terms of accuracy; however, the ensemble spread of ICEA prediction was found to be too narrow to cover the range of streamflow observations [*He et al*., 2012]. IEELA couples an ensemble-based MAP estimation with the lag-aware EnKS to assimilate discharge for streamflow forecasting. It addresses both the time lag issue and the error estimation issue in an integrated DA system. It was found to generate reliable ensemble spreads and effectively improve the discharge forecasts [*Li et al*., 2014]. So far applications of both ICEA and IEELA have been limited to lumped catchment modeling. Adapting these integrated DA approaches to address the challenges in distributed/semidistributed model updating remains an important scientific question.

Although lumped models may work well in small catchments, in many cases, especially in the operational flood forecasting systems, semidistributed models (i.e., distributed conceptual models) are preferred to make full use of distributed forcing information and multiple discharge gauges. In addition, there is a trend to move toward semidistributed/distributed catchment hydrologic modeling systems [*Lee et al*., 2012; *Rakovec et al*., 2012]. A number of studies have implemented DA schemes for distributed/semidistributed model updating [*Lee et al*., 2012; *McMillan et al*., 2013; *Noh et al*., 2011; *Rakovec et al*., 2012; *Ricci et al*., 2011].

Implementation of DA schemes in semidistributed systems requires additional consideration for parameterization/estimation of the error between subcatchments with spatial and temporal correlations. For temporal correlation, independent forcing and state errors have been preferred in many of previous studies [*Lü et al*., 2013; *Pauwels and De Lannoy*, 2009; *Wang et al*., 2009; *Weerts and El Serafy*, 2006; *Xie and Zhang*, 2010]. Ignoring autocorrelation of the error may, however, lead to underestimation of the ensemble spread and this becomes worse as the temporal modeling resolution increases (e.g., hourly forecasting) [*Li et al*., 2014; *McMillan et al*., 2013; *Rakovec et al*., 2012]. In addition, spatially uniform [*Thirel et al*., 2010a, 2010b] and spatially independent [*Salamon and Feyen*, 2009; *Xie and Zhang*, 2010] errors have both been used frequently in distributed system updating. It is likely that these idealized assumptions of spatial and temporal independence in error structure are unrealistic, which would lead to suboptimal performance of the DA system. This has been partially addressed by a few previous studies which have subjectively specified both temporal and spatial correlations of the model error [*Clark et al*., 2008; *McMillan et al*., 2013].

Even with the spatiotemporally distributed (and correlated) error specifications, superiority of a distributed/semidistributed model compared with a lumped model in combination with the discharge DA remains

uncertain when only the outlet discharge is available. Understanding this relative merit between distributed/semidistributed systems and lumped systems is essential for flood forecasting. Even though a few studies have implemented novel DA methods with distributed/semidistributed models [*Lee et al*., 2011, 2012; *McMillan et al*., 2013; *Rakovec et al*., 2012; *Xie and Zhang*, 2010], direct comparison of DA performance for lumped versus semidistributed systems was not provided.

Related to this issue, it is often presumed that internal system states/fluxes—for a semidistributed catchment system, soil water store, and discharge in the upstream subcatchments—are properly updated and improved after the discharge DA; however, the opposite results have been reported. Several studies have revealed that updating multiple subcatchments with a limited number of (i.e., fewer) discharge gauges may not improve, and can even cause deterioration in, discharge predictions at ungauged locations [*Clark et al*., 2008; *Lee et al*., 2011, 2012]. This is due to the hydrological systems typically being underdetermined [*Lee et al*., 2012] together with imperfect representation of physical processes and their uncertainties [*Clark et al*., 2008]. *Clark et al*. [2008] and *Lee at al*. [2012] discussed a need to develop appropriate models and DA tools to address these issues.

In extending IEELA to a semidistributed forecasting system in this study, the MAP estimation is used to quantify model and observation errors with the consideration of temporal and spatial correlations of the model error. The estimated error parameters are implemented with the lag-aware EnKS to address the errors in the initial conditions. The results are evaluated in hypothetical forecasting using observed forcing data with the lead time of 1–48 h. The results are analyzed to understand (1) whether there is any benefit of using a semidistributed catchment system compared with a lumped system in the context of DA; and (2) whether more realistic representation of the error propagation and more adequate correction of both current and antecedent errors (e.g., IEELA) results in improved discharge error correction in the ungauged locations.

2. Methodology

In this study, an hourly semidistributed flood forecasting system based on coupling the GR4H rainfall runoff model (modèle du Génie Rural à 4 paramètres Horaire) with a linear Muskingum river routing model is applied to the upper part of the Ovens River basin in Australia. The model parameters are calibrated using the shuffled complex evolution (SCE-UA) approach [*Duan et al*., 1992]. After the model calibration is completed, SCE-UA is used again to estimate the model and observational error parameters based on the MAP.

The EnKS is implemented for the following two scenarios: (1) updating the catchment states only (i.e., GR4H states), and (2) updating both the catchment states and the river routing states (i.e., both GR4H and Muskingum states). To examine any additional improvements made by using semidistributed model, results are compared with those from a lumped catchment configuration as presented by *Li et al*. [2014].

2.1. Catchment and Data

The study catchment is located upstream of Myrtleford in the Ovens River basin, Australia (Figure1). The catchment is about 1210 km^2 and mainly covered by eucalyptus forest. The main stream drains from the southeast to the northwest with a travel time of approximately 1 day. The mean annual rainfall and discharge are approximately 1170 and 440 mm, respectively. The major flows normally occur in July–October.

Data used in this study include hourly rainfall depth, potential evapotranspiration (PET), and gauged stream discharge for 1999–2010. Gauged rainfall data are spatially interpolated to subcatchments from 14 rainfall gauges using an inverse distance weighted approach [*Pagano et al*., 2011b]. The PET is monthly observed data extracted from Australian Water Availability Project (AWAP) products [*Raupach et al*., 2009, 2012]. There are five discharge gauges located at Harrietville, Bright, Harris Lane, Eurobin, and Myrtleford within the catchment. The purpose of this study is to investigate the effect of using a semidistributed model for DA applications when only the outlet discharge data are available, therefore, only discharge at Myrtleford (station code: 403210) is used for model calibration, error estimation, and DA. To avoid higher level of underdetermination in the modeling system and to make the reporting of results and analyses more concise, only two internal discharge gauges are used for the evaluation of potential improvements in internal "ungauged" sites by assimilating the outlet discharge. These were observations at Bright (station code: 403205) and Harris Lane (station code: 403233).

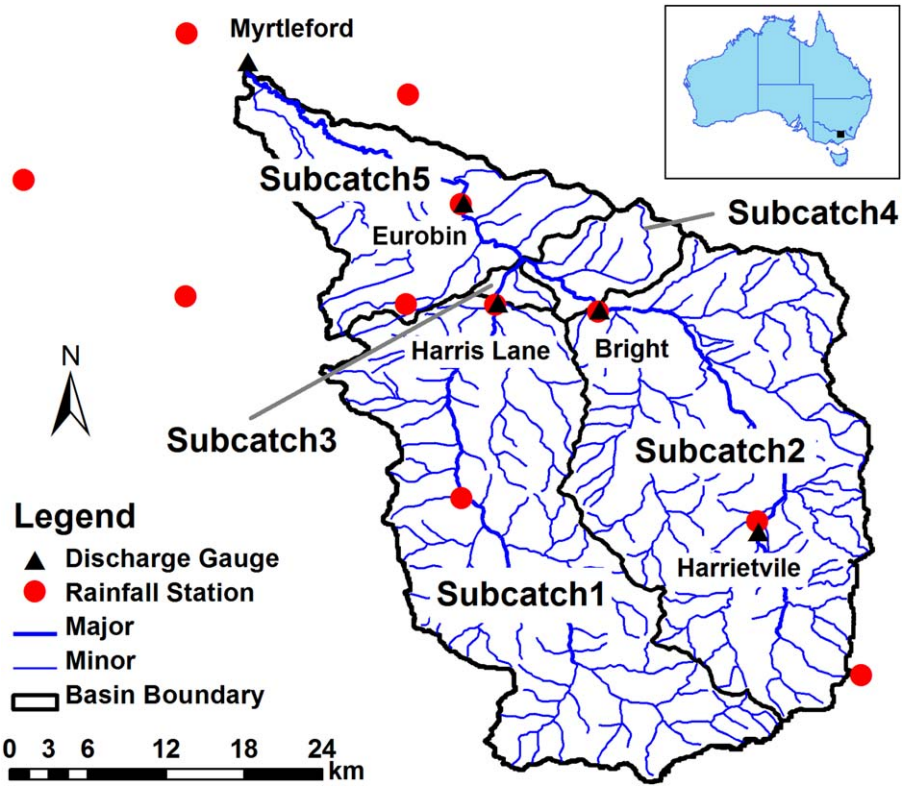

Figure 1. Study basin and subcatchments.

2.2. Semidistributed Model Setup and Calibration

Based on the gauge locations and the topography, the catchment is divided into five subcatchments: Subcatch1—upstream of Harris Lane, Subcatch2—upstream of Bright, Subcatch3—downstream of Harris Lane, Subcatch4—downstream of Bright, and Subcatch5—upstream of Myrtleford (Figure1). Runoff in each subcatchment is generated and preliminary routed to the outlet of the subcatchment using GR4H, while flows through the channel network are routed using a linear Muskingum channel routing model. The GR4H-estimated runoff is added into the channel network at the outlet of each subcatchment.

2.2.1. GR4H Rainfall Runoff Model

GR4H is an hourly version of the widely used daily catchment runoff generation model GR4J (modèle du Génie Rural à 4 paramètres Journalier). It is one of the main candidates in the Australian Bureau of Meteorology operational flood forecasting system and it has been found to work well in operational scenarios [*Li et al*., 2014; *Pagano et al*., 2010, 2011a].

GR4H is a storage-unit-hydrograph-based conceptual model (Figure 2), which means that both routing storages and unit hydrographs are used to create time delay in the runoff process. The throughfall (*Pn*) is divided into direct runoff (*Pn-Ps*) and infiltration (*Ps*) through a conceptual soil water store (*S*) with the maximum capacity of x_1. The direct runoff and percolation water are combined into a hillslope-scale total runoff (*Pr*), which is then split into two parts using a fixed ratio (1:9). One part (10% of *Pr*) is routed by a unit hydrograph (*UH*2) with length $2{\cdot}x_4$ (a fast catchment-scale routing), and the other part (90% of *Pr*) is routed by a cascade of one unit hydrograph (*UH*1) with length of x_4 and one routing store (*R*) with the "reference" capacity of x_3 (a slow catchment-scale routing). $F(x_2)$ nominally represents water exchange between the simulated catchment and adjacent catchments, with the maximum exchange rate of x_2.

2.2.2. The Linear Muskingum Routing Model

Runoff entering the stream network is routed using a linear Muskingum channel routing model. The Muskingum method is a finite-difference approximation of the Saint-Venant equations. It incorporates the concept of a triangular "wedge" and rectangular "prism" to represent storage in the river channel and flood

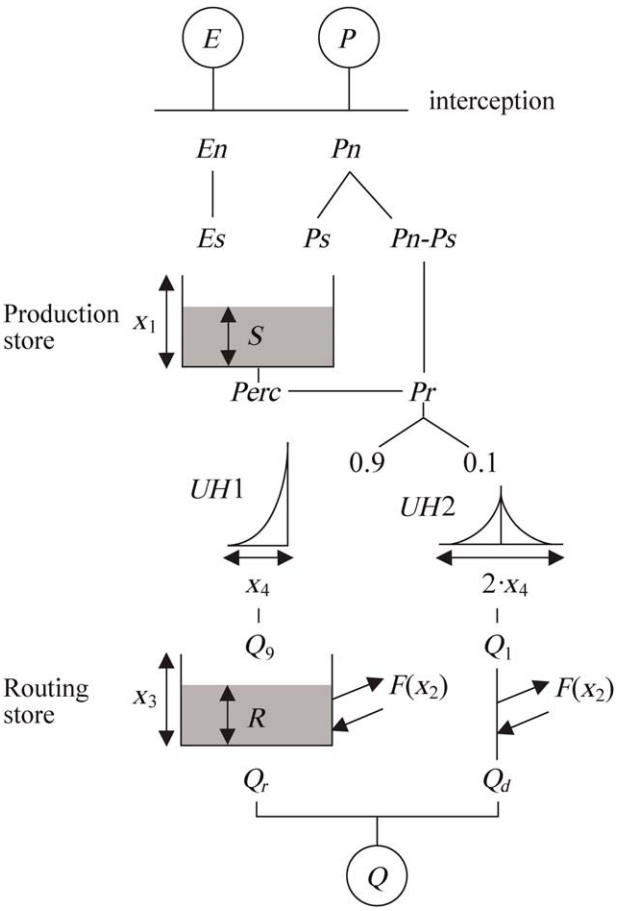

Figure 2. The structure of the GR4H model [*Li et al.*, 2013].

wave [*Cunge*, 1969; *Nash*, 1959]. Its linear form is based on mass conversation (continuity) and a linear storage which can be expressed as

$$\frac{dV_t}{dt} = I_t - O_t \quad \text{(Continuity/mass equation)}, \tag{1}$$

$$V_t = k \cdot [\omega \cdot I_t + (1-\omega) \cdot O_t] \quad \text{(Storage equation)}, \tag{2}$$

where V_t, I_t, and O_t are storage, inflow, and outflow at time t, respectively; k is a constantratio between storage and flow and ω is a weighting coefficient describing the relative significance of inflow and outflow to the storage.

2.2.3. Model Calibration

The semidistributed model, with four parameters (x_1, x_2, x_3, and x_4) from GR4H and two parameters (k and ω) from the Muskingum model, is calibrated against the Myrtleford discharge gauge at the catchment outlet. To avoid potential equifinality due to overparameterization, calibrated parameters in operational forecasting are usually set to be spatially uniform and only measureable parameters are allowed to vary between subcatchments [*Khakbaz et al.*, 2012; *Lee et al.*, 2012; *McMillan et al.*, 2013]. To be consistent with the operational applications, here parameters are set to be spatially uniformin this study, except for the length parameter (x_4) for the two unit hydrographs in GR4H. It has been shown that the concentration time of Australian catchments can be expressed as a power function of catchment area [*Li et al.*, 2013], therefore, x_4 is scaled by the square root of the subcatchment area to represent the flow concentration in this study. SCE-UA is used to identify the globally optimal parameter set. The objective function (equation (3)) used in this paper is an arithmetic average of a Nash-Sutcliffe model efficiency [*Nash and Sutcliffe*, 1970] of log flows (sensitive to low flows, equation (4)), a Nash-Sutcliffe model efficiency of Box-Cox transformed flows (sensitive to midrange flows, equation (5)), a Kling-Gupta Efficiency (sensitive to variance and high flows, equation (6)) [*Gupta et al.*, 2009], and a Bias skill score (equation (7)) [*Misirli et al.*, 2002].

$$F = F_{\log NS} + F_{BoxNS} + F_{KGE} + F_{bias}, \tag{3}$$

$$F_{\log NS} = \frac{\sum_{t=1}^{T_c} \left[\ln(Q_{sim,t}+v) - \ln(Q_{obs,t}+v)\right]^2}{\sum_{t=1}^{T_c} \left[\ln(Q_{sim,t}+v) - \ln(\bar{Q}_{obs,t}+v)\right]^2}, \tag{4}$$

$$F_{BoxNS} = \frac{\sum_{i=1}^{T_c} \left(Q'_{sim,t} - Q'_{obs,t}\right)^2}{\sum_{i=1}^{T_c} Q'_{sim,t}\left(-\bar{Q}'_{obs}\right)^2}, \tag{5}$$

$$F_{KGE} = 1 - \sqrt{(1-r)^2 + (1-\frac{\sigma_{sim}}{\sigma_{obs}})^2 + (1-\frac{\bar{Q}_{sim}}{\bar{Q}_{obs}})^2}, \tag{6}$$

$$F_{bias} = \left[\max\left(\frac{\bar{Q}_{sim}}{\bar{Q}_{obs}}, \frac{\bar{Q}_{obs}}{\bar{Q}_{sim}}\right) - 1\right]^2, \quad (7)$$

where $Q_{sim,t}$ and $Q_{obs,t}$ denote the simulated and observed discharges, respectively, at time t within the calibration period T_c; v denotes the smallest nonzero observed discharge of the calibration period; r denotes the correlation coefficient between simulated and observed discharges; $Q'_{sim,t}$ and $Q'_{obs,t}$ denote the Box-Cox transformed discharge through:

$$Q' = \frac{(Q+1)^{\gamma} - 1}{\gamma}. \quad (8)$$

where the transformation parameter γ is set to be 0.3, giving a score that is considered a good measure of intermediate flows [*Misirli et al*., 2002; *Pagano et al*., 2011b]. An evaluation for the study case here shows that the Box-Cox transformation with $\gamma = 0.3$ normalizes the discharge data to a large extent.

2.3. Error Structure and Estimation

The performance of an EnKS/EnKF is to a large extent determined by how well the model and observation errors are represented. They are used to reanalyze the model predictions by calculating a weighted average of the predictions and the observations (i.e., discharge in this study), where the weight coefficients are calculated based on the comparison between prediction and observation errors. Then model states (or parameters) are updated through the cross-covariance between the errors in the states and the errors in the predictions.

To construct a realistic error covariance matrix for the states and predictions, input rainfall (P) and catchment soil moisture (S) are perturbed to generate an ensemble of model states and discharge predictions (Q). Observed discharge is perturbed to represent the observation error. The uncertainties from *PET*, model parameters, and structure are assumed to accumulate in soil moisture thus they are represented by the perturbation of soil moisture. The error models used to reproduce rainfall, soil moisture, and discharge observation uncertainties, and a MAP as a method to estimate the error parameters [*Li et al*., 2014; *Sorenson*, 1980] are described in the following sections.

2.3.1. Rainfall Error

Rainfall uncertainty is one of the main sources of the prediction uncertainty. The rainfall error is in part directly propagated into discharge through direct runoff and its routing process, and the other part affects discharge error through soil moisture and base flow processes. Therefore, it is necessary to perturb rainfall independently of state perturbations, to generate more realistic ensemble propagation. A lognormal multiplicative error model has been broadly used for rainfall perturbation [*Crow et al*., 2011; *DeChant and Moradkhani*, 2012; *Nijssen and Lettenmaier*, 2004]; however, most of these implementations have not considered the temporal and spatial correlations of the rainfall error, which have been shown to be important in hydrologic modeling [*Adams et al*., 2012] and DA [*McMillan et al*., 2011, 2013]. In space-time rainfall modeling studies, rainfall uncertainty has been found to be autocorrelated and is usually simulated through autoregressive (AR) or autoregressive-moving-average (ARMA) models [*Seed et al*., 1999, 2000; *Smith and Krajewski*, 1991]. The spatial variability is usually quantified through either parametric methods, e.g., Kriging methods with exponential [*Krajewski*, 1987], Gaussian [*Sun et al*., 2000] or spherical covariance models [*Berne et al*., 2004], or nonparametric methods, e.g., the fast Fourier transform method [*Velasco-Forero et al*., 2009]. These methods, however, have not been widely implemented in hydrologic DA applications.

In this paper, we extend the first-order autoregressive lognormal model, namely AR(1)-LN, which was used by *Li et al*. [2014] for rainfall perturbation, to a spatially correlated autoregressive error model. In this model, stochastic rainfall for the subcatchment i at time t is generated by

$$P'_{i,t} = \xi^{P}_{i,t} \cdot P_{i,t}, \quad (9)$$

where the multiplier $\xi^{P}_{i,t}$ follows a lognormal distribution with a mean of 1 (unbiased perturbation) and standard deviation of ε_P. The natural logarithm of $\xi^{P}_{i,t}$ follows a first-order autoregressive process,

$$LN(\xi_{i,t}^{P}) = \mu + \alpha \cdot (LN(\xi_{i,t-1}^{P}) - \mu) + \delta_{i,t}^{P} \cdot \sigma \cdot \sqrt{1-\alpha^2}, \tag{10}$$

where α is the lag-one autocorrelation coefficient, μ and σ are the mean and the standard deviation of the Gaussian distribution followed by $LN(\xi^{P})$ and can be expressed as

$$\mu = -\frac{1}{2}\ln(1+\varepsilon_P{}^2), \tag{11}$$

$$\sigma = \sqrt{\ln(1+\varepsilon_P{}^2)}, \tag{12}$$

and $\delta_{i,t}^{P}$ is a standard Gaussian noise added to the subcatchment i at time t, which is resampled from a zero-mean joint probability distribution with the covariance matrix of

$$\mathbf{\Sigma}^{P} = \begin{bmatrix} 1 & \rho_{1,2}^{P} & \cdots & \rho_{1,I}^{P} \\ \rho_{2,1}^{P} & & & \vdots \\ \vdots & & \ddots & \\ \rho_{I,1}^{P} & \cdots & & 1 \end{bmatrix}_{I\times I}, \tag{13}$$

where $\rho_{i,j}^{P}$ is the covariance (also the correlation coefficient) between the standard Gaussian noises of subcatchments i and j. Instead of using independent $\rho_{i,j}^{P}$, we assume that the spatial correlation decreases exponentially with the increasing separation distance of the subcatchment centroids, which is

$$\rho_{i,j}^{P} = \exp\left(-\frac{d_{i,j}}{d_0^{P}}\right), \tag{14}$$

where $d_{i,j}$ is the distance between the centers of subcatchments i and j, and d_0^{P} is a reference distance.

In this model, there are three parameters that need to be estimated: the lag-one autocorrelation coefficient α, the standard deviation of rainfall multipliers ε_P, and the reference distance for spatial correlation d_0^{P}.

2.3.2. Soil Moisture Error

Catchment hydrologic models simulate soil moisture through the state transfer function, which can be simply formulated as

$$\mathbf{x}_t = f(\mathbf{x}_{t-1}, \mathbf{u}_t, \boldsymbol{\theta}), \tag{15}$$

where $\mathbf{x}$ is the state vector, $\mathbf{u}$ is the input variable vector, and $\boldsymbol{\theta}$ is the parameter vector. Soil moisture is a key state variable in a hydrologic model. According to equation (15), the soil moisture at time t is calculated based on the antecedent soil moisture at time $t-1$, and errors added to soil moisture will be accumulated in time. Therefore, perturbing soil moisture through temporally independent errors will result in a temporally correlated error in soil moisture. In this study, a spatially correlated and serially independent additive Gaussian noise is used to represent the soil moisture uncertainty:

$$S'_{i,t} = S_{i,t} + \xi_{i,t}^{S}, \tag{16}$$

where $\xi_{i,t}^{S}$ is a Gaussian noise calculated as

$$\xi_{i,t}^{S} = \varepsilon_S \times \delta_{i,t}^{S}, \tag{17}$$

where ε_S is the standard deviation of $\xi_{i,t}^{S}$ and $\delta_{i,t}^{S}$ is a standard Gaussian noise which is resampled from a zero-mean joint probability distribution with the covariance matrix of

$$\mathbf{\Sigma}^{S} = \begin{bmatrix} 1 & \rho_{1,2}^{S} & \cdots & \rho_{1,I}^{S} \\ \rho_{2,1}^{S} & & & \vdots \\ \vdots & & \ddots & \\ \rho_{I,1}^{S} & \cdots & & 1 \end{bmatrix}_{I\times I}, \tag{18}$$

and the spatial correlation coefficients ($\rho_{i,j}^{S}$) are calculated by the distance between the subcatchment centroids($d_{i,j}$) as

$$\rho_{i,j}^{S}=\exp\left(-\frac{d_{i,j}}{d_0^S}\right), \tag{19}$$

where d_0^S is the reference distance for the spatial correlation of soil moisture.

The perturbed soil moisture ($S'_{i,t}$) is truncated by the upper and the lower bounds of soil moisture. Two error parameters for soil moisture perturbation, the standard deviation ε_S and the reference distance for spatial correlation d_0^S, need to be estimated.

2.3.3. Discharge Error

Li et al. [2014] analyzed flow gauging data at Myrtleford and the discharge error was found to follow a Gaussian error (ξ^Q) accounting for heteroscedasticity:

$$Q'_t=Q_t+\xi_t^Q\cdot Q_t, \tag{20}$$

where ξ^Q is Gaussian noise with zero mean and a standard deviation of ε_Q.

According to the flow gauging data analysis by *Li et al.* [2014], ε_Q is estimated to be normally distributed with a mean of 9.25% and standard deviation of 0.925%. This estimated distribution of ε_Q is used as an a priori distribution to constrain the MAP estimation.

2.3.4. Maximum A Posteriori Error Estimation

Based on the assumed error structure, six error parameters need to be estimated: the standard deviations of the soil moisture error (ε_S), the standard deviation of the observed discharge multiplier (ε_Q), the standard deviation of the rainfall multiplier (ε_P), the lag-one autocorrelation coefficient of rainfall multiplier (α), the spatial correlation reference distances of rainfall multiplier (d_0^P), and soil moisture error (d_0^S). The three standard deviations are assumed to be the same for all subcatchments. An ensemble-based MAP estimation method constrained by the a priori distribution of ε_Q is used to estimate these error parameters.

MAP is a regularization of the maximum likelihood estimation, but incorporates a priori distributions over unknown parameters [*Li et al.*, 2014]. In this study, MAP provides a point estimation of model error parameters $\boldsymbol{\Theta}$ that maximizes its posterior probability density conditional on the model parameters $\boldsymbol{\theta}$, observed discharge (Q_{obs}), precipitation (P) and *PET* for all t within the calibration period (t_0–t_c). More specifically, it finds $\boldsymbol{\Theta}$ that maximizes

$$p(\boldsymbol{\Theta}|Q_{obs,\,t_0\to t_c};\boldsymbol{\theta},P_{t_0\to t_c},PET_{t_0\to t_c})\propto L(\boldsymbol{\Theta})=p(\boldsymbol{\Theta})\times\prod_{t=t_0}^{t}p(Q_{obs,\,t}|\boldsymbol{\Theta};\boldsymbol{\theta},P_{t_0\to t},PET_{t_0\to t}), \tag{21}$$

using a global optimization scheme; SCE-UA in this study. $L(\boldsymbol{\Theta})$ stands for the a posteriori likelihood of $\boldsymbol{\Theta}$. As catchment hydrologic processes are usually highly nonlinear, it is unrealistic to analytically derive the probability density of discharge from the probability distribution of inputs and states. Therefore, the error parameter calibration is conducted using a Monte Carlo approach, which generates an ensemble of realizations to represent the propagation of the probability distribution. More details about the procedure of the ensemble-based MAP estimation can be found in *Li et al.* [2014].

2.4. The Ensemble Kalman Smoother

The EnKS is implemented in an iteration of two steps: model prediction and state updating. The model prediction can be expressed as a state transfer process

$$\mathbf{x}_t^{i-}=f(\mathbf{x}_{t-1}^{i+},\mathbf{u}_t^i,\boldsymbol{\theta})+\boldsymbol{\omega}_t^i\quad i=1,\ 2\ \ldots\ n, \tag{22}$$

and an observation operator module

$$\hat{\mathbf{y}}_t^i=h(\mathbf{x}_t^{i-},\boldsymbol{\theta}), \tag{23}$$

or

$$\hat{\mathbf{y}}_t^i=h(\mathbf{x}_{t\to t-m+1}^{i-},\boldsymbol{\theta}), \tag{24}$$

where $\mathbf{x}^{i-}$ represents the predicted state vector, $\mathbf{x}^{i+}$ the updated state vector, $\boldsymbol{\omega}^i$ the error vector added to states (i.e., the soil moisture error parameterized through equation (16) in this case), $\hat{\mathbf{y}}^i$ the observational

prediction vector (discharge in this case), t the current time step, m the lagged time steps contributing to the current prediction, and i enumerates a member of a size-n ensemble.

In the case where discharge data are assimilated, equations (23) and (24) represent the calculation of the discharge prediction ($\hat{\mathbf{y}}^i$) based on the model water storages ($\mathbf{x}^{i-}$). When the runoff routing is based on dynamic storage(s), the discharge predicted using the current routing stores through equation (23). In this case, the real-time EnKF can effectively correct the model state errors by assimilating discharge [*Li et al*., 2013]. However, if runoff routing is fully or partially based on unit hydrographs, the discharge prediction is made based on a series of catchment states within a lagged time window of length m as in equation (24). For the latter type of models, the lag-aware EnKS has proved to be superior to the nonlag-aware EnKF [*Li et al*., 2013].

As the subcatchment routing of the GR4H model is partially based on unit hydrographs, the EnKS with a fixed time window is used. In the state updating step, the EnKS updates the current and antecedent states via

$$\mathbf{x}^{i+}_{t\to t-k+1}=\mathbf{x}^{i-}_{t\to t-k+1}+\mathbf{K}^*_t(\mathbf{y}^i_t-\hat{\mathbf{y}}^i_t), \tag{25}$$

$$\mathbf{y}^i_t=\mathbf{y}_t+\boldsymbol{\eta}^i_t, \tag{26}$$

where $\mathbf{y}_t$ is the observation vector; $\mathbf{y}^i_t$ is the perturbed observation vector; $\boldsymbol{\eta}^i_t$ is the observation error, which is parameterized following equation (20); k is the size of the fixed updating time window, which should be equal to or larger than the lagged time window m in equation (24). The Kalman gain matrix $\mathbf{K}^*_t$ can be calculated as

$$\mathbf{K}^*_t=\boldsymbol{\Sigma}^{xy*}_t[\boldsymbol{\Sigma}^{yy}_t+\boldsymbol{\Sigma}^{y}_t]^{-1}, \tag{27}$$

where $\boldsymbol{\Sigma}^{yy}_t$ is the error covariance matrix of the observational predictions; $\boldsymbol{\Sigma}^{y}_t$ is the error variance matrix of the observations; and $\boldsymbol{\Sigma}^{xy*}_t$ is the cross covariance matrix of all the state variables within the updating time window and current observational predictions:

$$\boldsymbol{\Sigma}^{xy*}_t=\left(\boldsymbol{\Sigma}^{x_t y}_t,\boldsymbol{\Sigma}^{x_{t-1} y}_t,\cdots,\boldsymbol{\Sigma}^{x_{t-k+1} y}_t\right)^T. \tag{28}$$

where $\boldsymbol{\Sigma}^{xy}_t$ is the cross covariance matrix of the state variables and observational predictions.

2.5. Evaluation Methods

The *BIAS* and the Nash Sutcliffe model efficiency coefficient (*NS*), shown in equations (29) and (30), are used to evaluate the accuracy of mean forecasts:

$$BIAS=\frac{1}{L}\sum_{t=1}^{L}(Q_{fcst,t}-Q_{obs,t}), \tag{29}$$

$$NS=1-\frac{\sum_{t=1}^{L}(Q_{fcst,t}-Q_{obs,t})^2}{\sum_{t=1}^{L}(Q_{obs,t}-\bar{Q}_{obs})^2}, \tag{30}$$

where $Q_{fcst,t}$ denotes the mean of an ensemble forecast discharge at time t, $Q_{obs,t}$ the observed discharge at time t, $\bar{Q}_{obs}$ the temporal mean of the observed discharge time series, and L the length of the evaluation period.

The ensemble forecast skill is evaluated by the temporal mean of ensemble root mean squared error (*MRMSE*), the continuous ranked probability score (CRPS), and the rank histogram. The *MRMSE* calculates the *RMSE* at each time step using all ensemble members then averages the *RMSE*s for the entire evaluation period [*Li et al*., 2013] as follows:

$$MRMSE=\frac{1}{L}\sum_{t=1}^{L}\sqrt{\frac{1}{N}\sum_{i=1}^{N}(Q^i_{fcst,t}-Q_{obs,t})^2}, \tag{31}$$

where $Q^i_{fcst,t}$ denotes the i-th member of an ensemble forecast discharge at time t, and N is the ensemble size. It is used as a measure to evaluate the accuracy of ensemble forecasts. The CRPS is a statistic

quantifying the closeness of the cumulative distribution functions (CDFs) of ensemble forecasts and the corresponding observations [*Candille and Talagrand*, 2005], which can be expressed as

$$CRPS = \frac{1}{L}\sum_{t=1}^{L}\int_{-\infty}^{\infty}\left(F_{fcst,t}(Q) - F_{obs,t}(Q)\right)^2 dQ, \tag{32}$$

where $F_{fcst,t}(Q)$ is the empirical cumulative distribution function (ECDF) of an ensemble forecast at time t; and $F_{obs,t}(Q)$ is the ECDF of the observation. As the deterministic observation is used, the ECDF of the observation can be expressed as

$$F_{obs,t}(Q) = \begin{cases} 0 & (Q < Q_{obs,t}) \\ 1 & (Q \geq Q_{obs,t}) \end{cases}, \tag{33}$$

which is also known as the Heaviside Step Function. The *CRPS* quantifies both the forecast accuracy and ensemble reliability in a single statistic. For a fixed mean forecast, either an excessively wide or narrow spread can lead to a large *CRPS*.

The rank histogram [*Hamill*, 2001] is also used to evaluate the overall reliability of the ensemble spread. To construct the rank histogram, N ensemble members in a forecast at time t are ranked in ascending order, and the forecast space is delineated into $N+1$ intervals (open-ended for the first and the last). The rank histogram illustrates the frequency of observations that fall into each interval. A flat rank histogram indicates that the ensemble spread is reliable for representing the real uncertainty. A U-shaped histogram indicates the spread is too narrow (i.e., underestimated forecast uncertainty). A concave downward histogram indicates the spread is too wide (i.e., overestimated forecast uncertainty), and an asymmetric histogram indicates a bias in the overall forecast.

3. Results and Discussion

The model parameters ($\boldsymbol{\theta}$) are calibrated for the period from 1 January 1999 to 21 July 2004, and the error parameters ($\boldsymbol{\Theta}$) are then estimated for the same calibration period. The EnKS is implemented to only the GR4H states for the EnKS-1 case, and to both GR4H and Muskingum states for the EnKS-2 case during the evaluation period from 22 July 2004 to 31 December 2010. The skills of the updating schemes are evaluated against the open-loop ensemble forecasting produced using perturbed observed forcing for the same evaluation period (i.e., 2005–2010) with lead times of 1, 6 12, 24, and 48 h. The ensemble size is 100. The system configuration for lumped modelling (EnKS-lumped case) is identical to that in *Li et al*. [2014], thus results from that study are used in this paper for comparison with the semidistributed modeling approach.

3.1. Model Calibration and Error Estimation

As the five subcatchments are calibrated simultaneously using the gauged discharge at Myrtleford (catchment outlet), the catchment and river routing parameters, except for x_4, are assumed to be identical in all subcatchments. A reference x_4 is set for a reference subcatchment with an area of 250 km^2, and is then scaled into individual x_4 values for each subcatchment by the square root of subcatchment area to represent the flow concentration time. Table 1 shows the calibrated model parameters. The conceptual soil moisture (S) has a maximum capacity (x_1) of 813 mm and the conceptual slow routing storage (R) has a reference capacity (x_3) of 49.6 mm. It should be noted that the slow routing is parameterized through the combination of *UH*1 and *R*, therefore, *R* only represents part of the of groundwater capacity. A negative x_2 (-1.58 mm) is conceptualized as a water exchange with (loss to) adjacent catchments in GR4H. The referencex_4 is 5.2 h, which is scaled to 7.3, 7.0, 2.3, 1.1, and 4.7 h for the five subcatchments, respectively. This means the largest subcatchment (Subcatch1) has the longest fast-routing delay of 7.3 $\times$ 2 h (the length of *UH*2 in Figure 2). However, x_4 only reproduces the time lag of the fast-routing process in subcatchment-scale. Runoff is later further delayed through the river routing process (Muskingum). The parameter ω in the Muskingum model is 0.9, which indicates that the outflow has much larger contribution to the conceptual nonlinear storage than the inflow (equation (2)).

Error parameters estimated by MAP using models described in section 2.3 are summarized in Table 2 (Case 1). The result suggests that the a posteriori estimation of the standard deviation of the discharge multiplier

Table 1. Calibrated Model Parameters

x_1 (mm)	x_2 (mm)	x_3 (mm)	x_4 (h)	k	ω
813	−1.58	49.6	5.2	0.9	0.2

is 0.1 (10% of discharge observation), which is very close to the a priori mean 0.0925 (9.25% of discharge observation). The rainfall multiplier has a standard deviation of 0.28 (28% of the rainfall amount), with the lag-one autocorrelation coefficient of 0.59. The error added to the soil moisture has a standard deviation of 1.58 mm, which is 0.19% of the maximum soil water capacity (x_1). As the rainfall-runoff model itself is a first-order Markov process, the error added will be accumulated in soil moisture, which leads to a temporally correlated soil moisture error with an adequate soil moisture ensemble spread.

The reference distances (d_0) of the spatial correlation of the rainfall and soil moisture errors are 595 km and 287 km, respectively, which are very large compared with some previous studies on rainfall spatial variability, e.g., the rainfall spatial correlation was found to be less than 0.3 when the distance increases to above 30 km [*Seed et al*., 2002; *Velasco-Forero et al*., 2009]. However, the correlation coefficients of rainfall and soil moisture errors areas high as 0.95 and 0.91 (Table 3), respectively, between Subcatch1 and Subcatch5, while the distance between the centroids of these two subcatchments is 27.4 km. This indicates that the spatial correlation may be overestimated due to the lack of error information from rainfall and soil moisture. As the hydrologic model is not physically based and the states and parameters are conceptualized, it may not be able to draw physically realistic error structure information from the integrated uncertainty in discharge.

3.2. Spatiotemporally Correlated Error Structure

To evaluate the influence of incorporating the spatial and temporal error correlations, three additional error parameterization schemes are examined by ignoring either the temporal (Case 2) or the spatial correlation (Case 3), or both the spatial and temporal correlations (Case 4). Error parameters are estimated using MAP for each case and are summarized in Table 2. As is expected theoretically, ignoring temporal or spatial error correlation or both leads to unrealistically higher variances in rainfall and/or soil moisture error estimates. For instance, the variance of multiplicative rainfall error of 0.42 in Case 4 is higher than previously reported values [*Li et al*., 2014; *Vrugt et al*., 2008]. This is because independent errors from upstream subcatchments or antecedent time steps tend to overly cancel each other while they propagate to the catchment outlet or to the current time step, consequently larger variance for individual errors is required to generate a sufficiently wide prediction spread at the catchment outlet.

Figure 3 illustrates the rank histograms of the open-loop ensemble forecasts at three evaluation points for the four error parameterization cases. All cases gives relatively reliable ensemble spread at the catchment outlet (Myrtleford) although Case 4 gives a slightly right skewed probability distribution, indicating a slight under estimation of the mean prediction. This similarity in reliability of the spreads at Myrtlefordis expected as the error parameters are estimated to maximize their a posteriori probability at the catchment outlet. However, the rank histograms (Figures 3b and 3c) also show that only Case 1 gives a reliable ensemble spread at the upstream locations (e.g., Bright and Harris Lane). The rank histograms at Bright and Harris Lane in the other three cases exhibit a convex shape, which means that the spreads are too wide (overpredicted). This supports the above conclusion that the error variances are overestimated when spatial and/or temporal error correlation is ignored. The overestimated errors then lead to overpredicted discharge spreads at the upstream gauges, but a reliable spread at the catchment outlet due to the high error variance in generation which is then compensated at the outlet by a stronger averaging effect.

3.3. The Benefit of Using A Semidistributed Model

The lag-aware EnKS was implemented for lumped model updating in the previous study by *Li et al*. [2014] using the same data set. Therefore, the results (EnKS-lumped) are directly comparable with the EnKS-1 (updating GR4H states only) and the EnKS-2 (updating GR4H and Muskingum states). Figure 4 compares the forecast statistics of semidistributed open-loop, lumped open-loop, EnKS-1, EnKS-2, and EnKS-lumped at Myrtleford.

Table 2. Estimated Error Parameters

	ε_P	ε_S (mm)	ε_Q	α	d_0^P (km)	d_0^S (km)
Case 1	0.28	1.58	0.10	0.59	595	287
Case 2	0.39	1.64	0.10	0	565	304
Case 3	0.33	2.37	0.11	0.57	0	0
Case 4	0.42	2.57	0.11	0	0	0

Comparison of the open-loop forecasts shows that the semidistributed model (dashed black curves) exhibits stronger

Table 3. Spatial Correlation Coefficient Matrices of Rainfall and Soil Moisture Errors (Case 1)

	Rainfall					Soil Moisture				
Subbasin	1	2	3	4	5	1	2	3	4	5
1	1	0.98	0.97	0.97	0.95	1	0.95	0.94	0.94	0.91
2		1	0.96	0.97	0.96		1	0.93	0.94	0.91
3			1	0.99	0.98			1	0.98	0.96
4				1	0.98				1	0.97
5					1					1

forecast skills than the lumped model (solid black curves) for all error metrics. The semidistributed model forecasts feature a smaller absolute *BIAS* and a higher *NS* coefficient compared with the lumped model forecasts, which indicates more accurate deterministic forecasts by the semidistributed model after calibration. In addition, smaller *MRMSE* and *CRPS* of semidistributed open-loop indicate that, after model calibration and error estimation, the semidistributed model generates more accurate and reliable ensemble forecasts than the lumped model.

As both the lumped and semidistributed models are calibrated against the Myrtleford flow gauge at the outlet of the catchment, the semidistributed model does not take advantages of any additional discharge data. In addition, as all five subcatchments share one set of model and error parameters, the use of semidistributed system does not significantly increase the degree of freedom of the model and error parameters, i.e., the total number of model and error parameters has only been increased from 8 to 12 (four additional parameters include two Muskingum parameters and two spatial correlation reference distances). Finally this comparison is for an independent validation period. Therefore, the improved skill of the semidistributed system must result from the use of spatially distributed input information, i.e., the rainfall and PET data and/or improved representation of routing.

Despite the noticeable improvement in open-loop forecasts using the semidistributed model, the DA makes the difference between the lumped and the semidistributed cases less significant. The *BIAS* indicates that the EnKS can effectively correct the over (lumped) or underestimated (semidistributed) forecasts for short lead times (i.e., several hour forecasts). For the longer lead times of 24–48 h, the forecast errors tend to be slightly overcorrected compared with the open-loop forecasts, i.e., corrected from the positively biased open-loop to the negatively biased forecasts in lumped model, and vice versa in the semidistributed model. Nevertheless, the biases in 48 h forecasts are still smaller than in the open-loop forecasts. For instance, the biases of the EnKS-1 and EnKS-2 are approximately 0.21 and 0.17 m^3/s at 48 h lead time, respectively, while the open-loop bias is -0.34 m^3/s. The difference in bias between EnKS-1/-2 and EnKS-lumped is negligible.

In terms of the *NS*, *MRMSE*, and *CRPS*, EnKS-2 performs better than EnKS-lumped, while EnKS-1 and EnKS-lumped perform similarly. More specifically, EnKS-2 exhibits a higher *NS* coefficient and lower *MRMSE* and *CRPS* than EnKS-lumped for all lead times. EnKS-1 tends to be worse than the EnKS-lumped at the beginning of forecasting (e.g., 1 h forecasts) but better for longer-term forecasts (e.g., 48 h forecasts) in terms of *NS* coefficient and MRMSE. Nevertheless, based on the comparison between EnKS-2 and EnKS-lumped, it is evident that the overall forecast skill can be improved by deploying a semidistributed model. The reason that the EnKS-1 is worse than the EnKS-2 is that the Muskingum routing is not directly updated in EnKS-1. The direct adjustment of the river routing (EnKS-2) should be more effective for forecast error reduction, especially at the beginning of the forecasts. In this study, model error is represented through perturbation of rainfall and soil moisture. But if additional error is added to the river routing module, the advantage of EnKS-2 compared with EnKS-1 would be more significant.

In summary, a semidistributed system can make better use of spatial forcing information compared with a lumped system, which results in more accurate open-loop forecasts. The superiority still exists after continuously assimilating observed discharge to update both rainfall-runoff and river-routing states, as demonstrated by the comparison between EnKS-2 and EnKS-lumped. However, it is also noted that the difference between EnKS-2 and EnKS-lumped is smaller than the difference between semidistributed open-loop and lumped open-loop. One reason is that there is more room for the open-loop of the

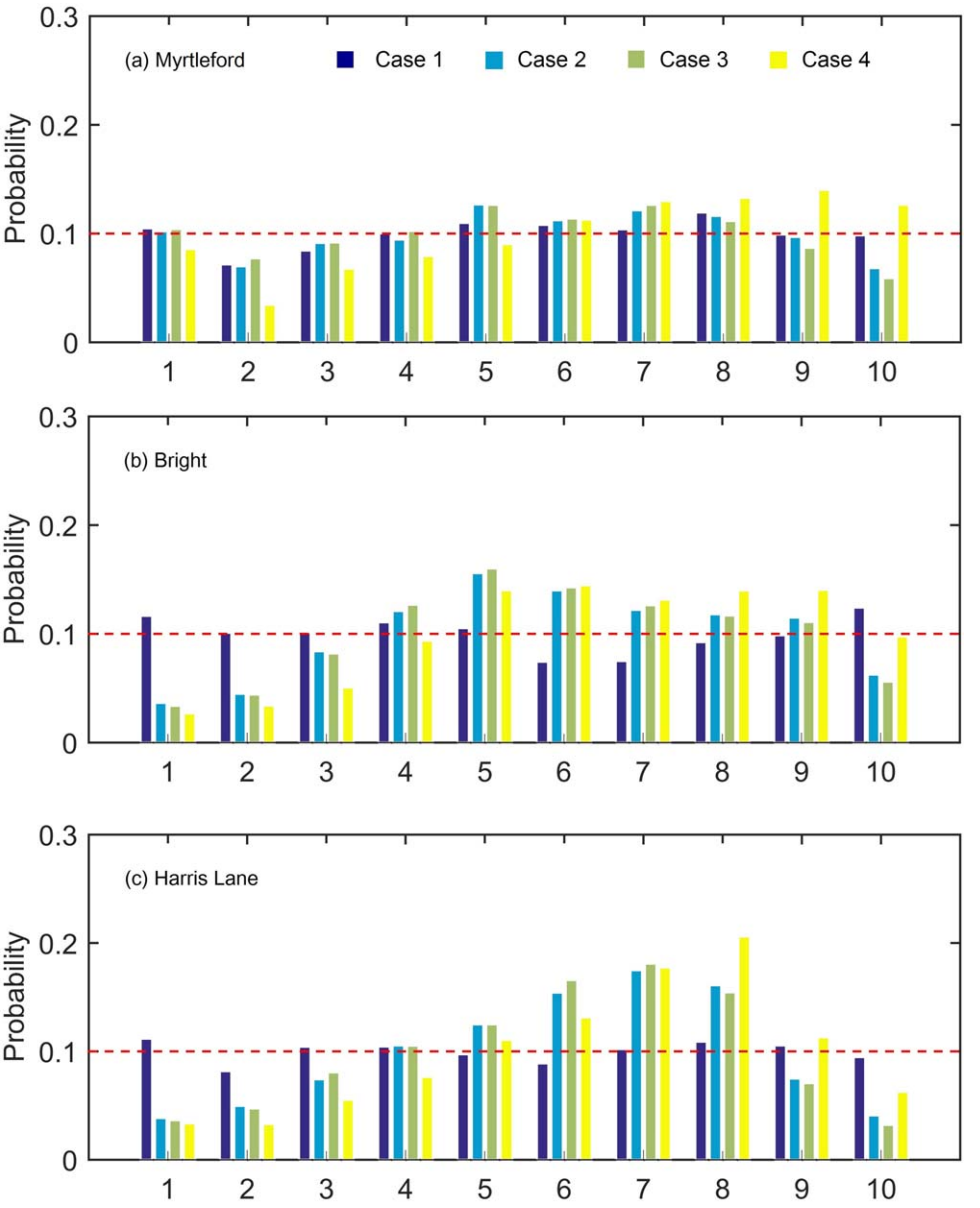

Figure 3. Rank histogram of the open-loop forecasts from 2005 to 2010 at (a) Myrtleford, (b) Bright, and (c) Harris Lane, respectively.

lumped model to be improved than for the semidistributed model. The efficacy of the EnKS, whether for the lumped or for semidistributed, is capped by the observational error, which was estimated previously. Another possible reason for the smaller improvement in the semidistributed DA cases is that while increasing the number of subcatchments makes better use of distributed forcing information, it also implies an increase in the degrees of freedom of the state space. The higher dimension of the state vector results in a more complex error covariance matrix, which may impair the efficiency of DA algorithms. Nevertheless, the overall performance of the updated semidistributed model is still better than that of the lumped model. Therefore, it is still worth applying a semidistributed/distributed system with a moderate spatial discretization (five subcatchments) instead of a lumped system even under DA scenarios. There are two caveats on this. (1) There needs to be sufficient spatially distributed information to improve the forecast performance, e.g., when there are sufficient rainfall gauges within and around the basin. (2) The error structures need to be properly estimated and adequately addressed through appropriate integrated DA scheme.

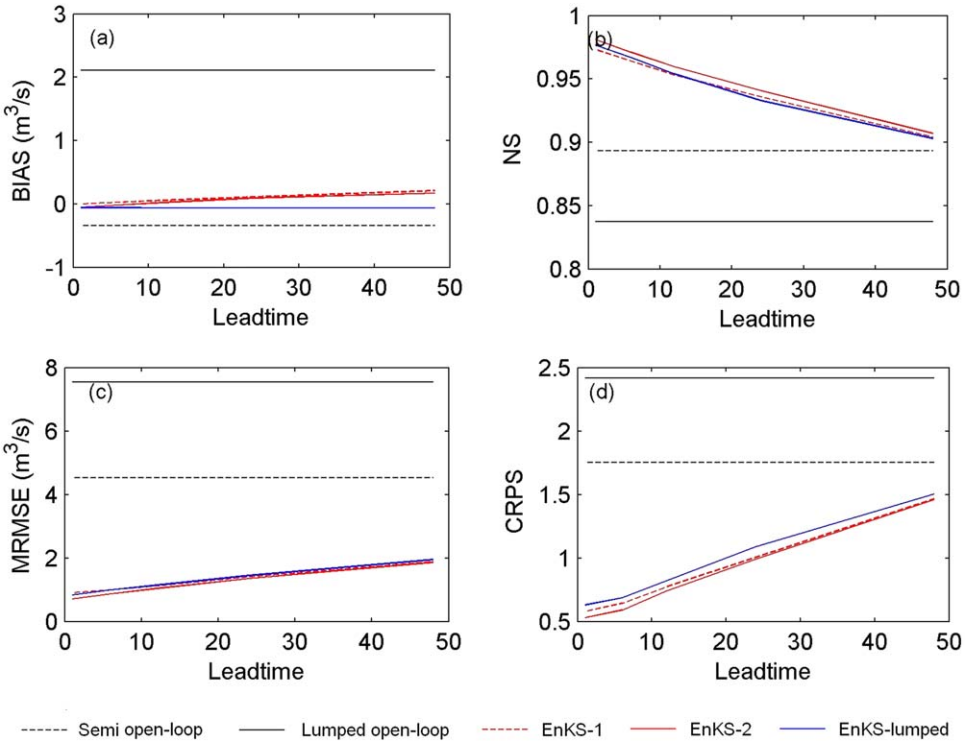

Figure 4. Statistics of forecasts at Myrtleford with the lead time up to 48 h (2005–2010).

3.4. System Performances in Ungauged Internal Area

As Bright and Harris Lane are assumed to be "ungauged," the discharge data at these gauges are used only for evaluation. Therefore, it remains uncertain whether the semidistributed model can produce accurate discharge predictions at Bright and Harris Lane. The calibrated model gives deterministic predictions for the calibration period (1999–2004) at Bright and Harris Lane with the *NS* model efficiency coefficients of 0.54 and 0.61, which are significantly lower than that at Myrtleford (0.91) as expected. However, as illustrated by the rank histogram in Figure 3, the ensemble spread at the upstream gauges (i.e., Bright and Harris Lane) are almost as reliable as the spread at Myrtleford. This indicates that the calibrated error models are reliable enough to represent the uncertainties at the internal gauges.

Figure 5 plots the *MRMSE* and *CRPS* of the forecasts after DA at Bright and Harris Lane. The EnKS-2 is shown to be better than the EnKS-1 at Bright, while the difference between these two is negligible at Harris Lane. Compared with the open-loop forecasts, the EnKS-2 has reduced the ensemble spread significantly, as the *MRMSE* decreases after state updating. However, the reduction of the spread does not necessarily represent an improvement in the accuracy since it can result in a reduced reliability of the ensemble forecasts. For instance, only the EnKS-2 gives a lower (better) *CRPS* at Bright for short lead times (1–12 h forecasts) compared with the open-loop case. It gives higher *CRPS* at Bright for longer-term forecasts, e.g., the 24–48 h forecasts, and higher *CRPS* at Harris Lane for all the lead times. Figure 6 and Figure 7 illustrate the ensemble spread of the EnKS-2 forecasts in 2009 at these two gauges, respectively. There exists obvious overestimation or underestimation after DA, indicating a degraded forecast skill of DA compared with the open-loop. These time series also indicate that the EnKS-2 has excessively reduced the spread, as a result, the forecast interval (95%) doesnot envelope observations effectively. However, it should be noted that the ensemble forecasts do not account for discharge observational uncertainties and the forecast interval is expected to envelope the truth, rather than the observations.

To sum up, the semidistributed catchment modeling in combination with MAP generated reliable ensemble forecasts at the ungauged subcatchment outlets even though the deterministic forecast accuracy (quantified by NS) is significantly lower that the accuracy at the gauged outlet. However, the forecast accuracy at the ungauged outlets was only occasionally improved or can even be degraded by assimilating the outlet

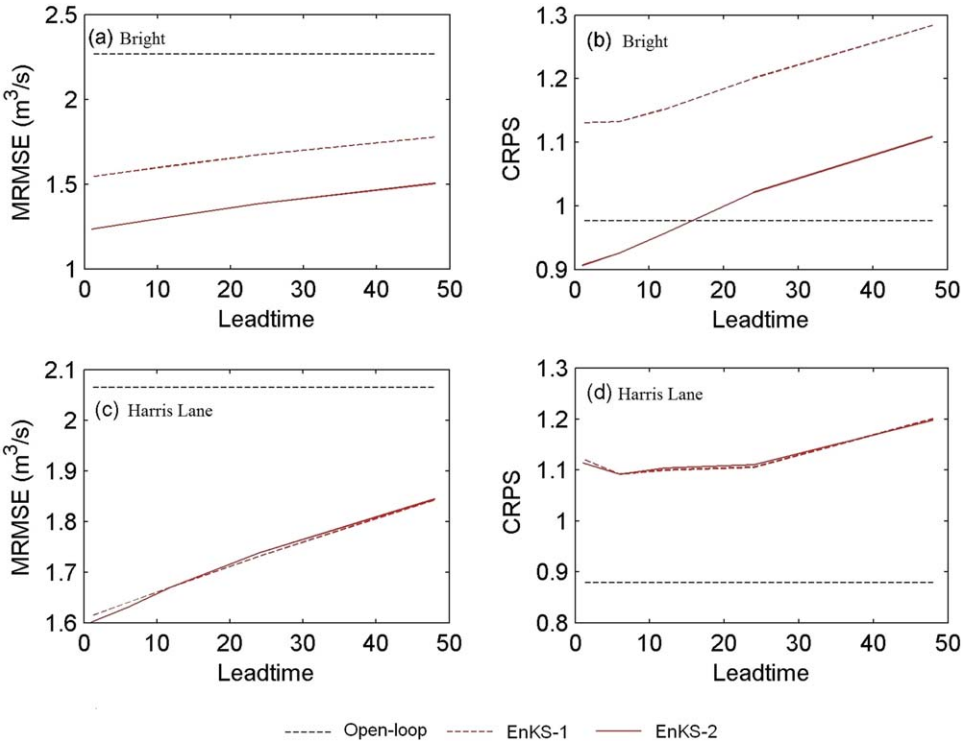

Figure 5. Statistics of forecasts at Bright (a and b) and Harris Lane(c and d) two internal locations with the lead time up to 48 h (2005–2010).

discharge data. The poor performance of DA at the ungauged outlets is associated with the fact that the rainfall-runoff model is not adjusted (i.e., calibrated and updated) against internal gauges. Similar degradation at internal sites has also been found by others. *Clark et al*. [2008] implemented a log-transformed ensemble square-root filter (EnSRF) with the TopNet model and found that assimilating discharge at the outlet gauge lead to similar forecast performance at one internal gauge and worse performance at two other internal gauges. *Lee et al*. [2012] also found that the forecasts in internal areas were degraded with 10% increase in the *RMSE* of the ensemble mean in 6 h forecasts. They concluded that the degradation was caused by the underdetermined system when outlet discharge data was assimilated to update the large number of states in the distributed model.

To address this issue, *Clark et al*. [2008] suggested improving the model physics and uncertainty estimation approach. *Lee et al*. [2012] pointed out that there is a need to develop appropriate DA tools to properly address the underdetermination issue. However, despite of a number of advanced distributed physically based models developed so far, it is difficult to build a model that can fully represent realistic hydrologic process and sources of uncertainties. Our results indicate that, even with better error representation combined with DA (i.e., IEELA), improvements at ungauged internal locations are not guaranteed. One important reason for this is that current flood forecasting systems are still mostly based on semidistributed models, i.e., distributed conceptual models, and the physical basis is still weak. Therefore, incorporating more data to constrain the model might be a more feasible solution. With the lack/absence of gauged discharge data, incorporating remote sensing data for model calibration and DA could be a viable approach. Some preliminary evidence can be found from *Zhang et al*. [2009].

4. Additional Results and Discussion

The efficacy of the lag-aware EnKS has been tested in a series of synthetic [*Li et al*., 2013] and real-time experiments [*Li et al*., 2014] for lumped streamflow modeling. However, considering that this is the first time the EnKS has been applied to a semidistributed/distributed model with MAP uncertainty estimation, we also conducted the two additional experiments using (1) the EnKF to update GR4H states (EnKF-1) and

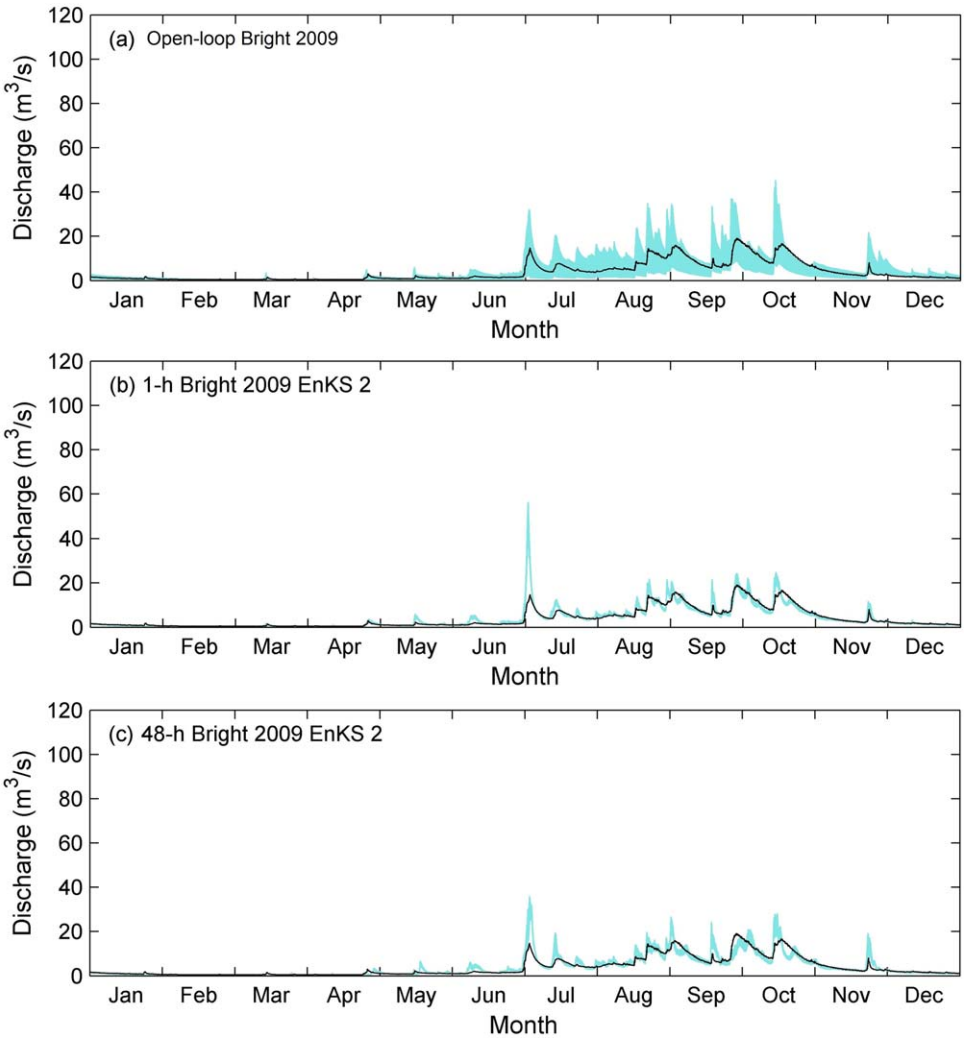

Figure 6. Ensemble spread of forecasts at Brightin 2009. Solid curves are observed discharge while cyan areas are the 95% confidence intervals of forecasts.

(2) the EnKF to update GR4H and Muskingum states (EnKF-2), to further investigate the merits of the EnKS on addressing time lag issue compared with the EnKF.

Figure 8 shows the *BIAS*, *NS*, *MRMSE*, and *CRPS* of discharge forecasts based on EnKF-1, EnKF-2, EnKS-1, and EnKS-2 with lead times of 1, 6, 12, 24, and 48 h. Generally speaking, all DA schemes improve the skill of the forecasting system, except for EnKF-1. The results solidify the superiority of the EnKS, e.g., EnKS-1 and EnKS-2 exhibit higher forecast skill than EnKF-1 and EnKF- 2, respectively. However, it is also interesting to find that EnKS-1 is significantly better than EnKF-1, while EnKS-2 is only slightly better than EnKF-2.

It has been reported that when the routing is not updated, the standard EnKF could result in unintended forecast errors such as the spurious peaks or oscillations, which can lead to worse overall accuracy [*Clark et al*., 2008; *McMillan et al*., 2013]. Using lag-aware DA schemes can, to a large extent, address this issue [*Li et al*., 2014; *McMillan et al*., 2013]. When a lumped model is used, the time lag is caused by the routing module, e.g., unit hydrographs [*Li et al*., 2014; *Pauwels and De Lannoy*, 2009], of a single catchment. When a distributed/semidistributed model is used, each subcatchment will cause a separate lag of flow and its error, which is then further lagged by the river routing module. In this case, the time lag issue is expected to be more complex and significant, e.g., *McMillan et al*. [2013] and EnKF-1 versus EnKS-1 in this study.However, it should be noted that when the river routing module is updated directly, this time lag issue should be reduced and the difference between the EnKF and the EnKS (EnKF-1 versus EnKS-2) can be less significant.

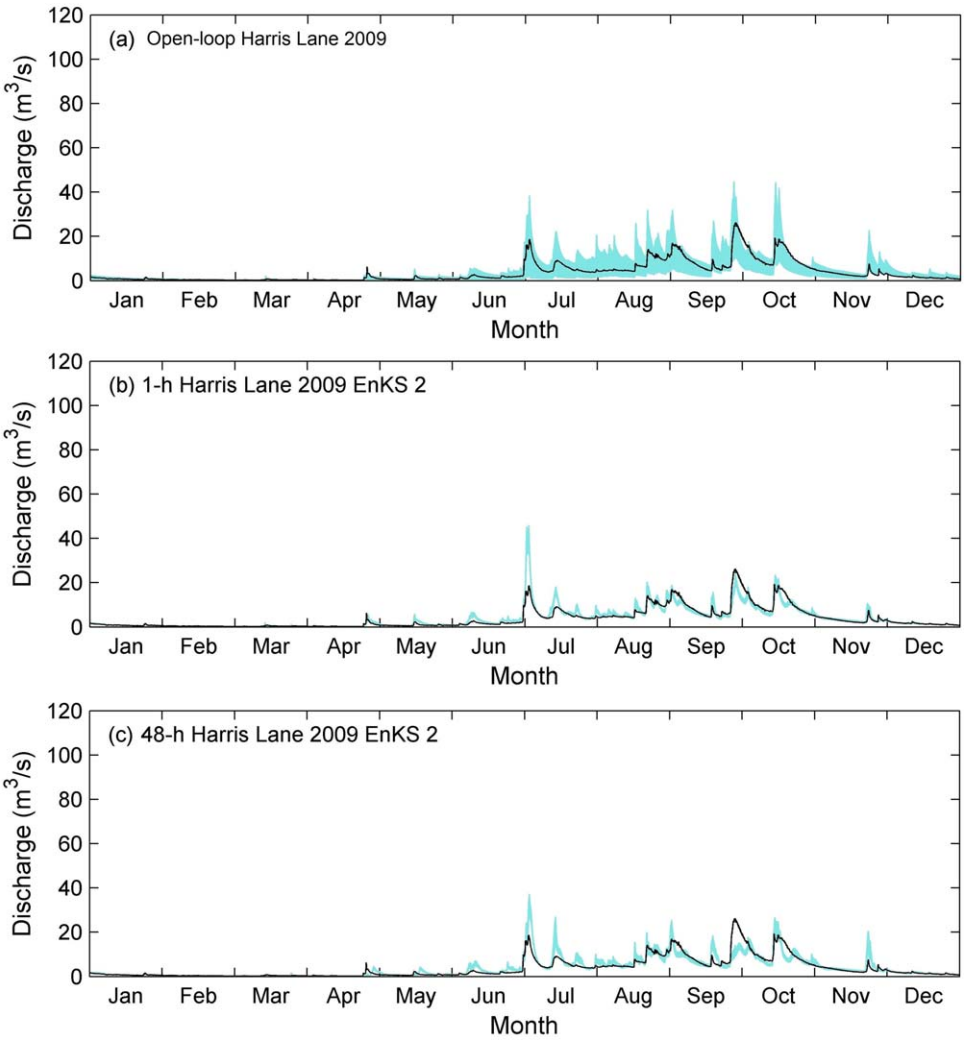

Figure 7. Ensemble spread of forecasts at Harris Lanein 2009. Solid curvesare observed discharge while cyan areas are the 95% confidence intervals of forecasts.

Prior to this work, there has been a number of studies related to time-lag issue in discharge DA [*Lee et al*., 2012; *Li et al*., 2013, 2014; *McMillan et al*., 2013; *Pauwels and De Lannoy*, 2009; *Rakovec et al*., 2012]. The consensus suggestion of these previous works is that, in hydrologic state updating, all "water," including catchment-stored water and routed water, should be updated. If the model is fully storage-based and the storages are accessible to DA techniques, "water" in all states should be updated directly [*Rakovec et al*., 2012]. If the catchment routing or river routing module cannot be updated directly by DA, a lag-aware DA approach, such as the EnKS [*Li et al*., 2013], the recursive EnKF [*McMillan et al*., 2013], or the variational DA [*Lee et al*., 2012], should be used so that the "water" conceptually retained in the routing modules could be indirectly updated through the model dynamics following updating of past states. The lag-aware approaches provide a way to achieve the objective of addressing errors in all "water."

From this point of view, it is explicable that the EnKF-2 is comparable with the EnKS-2 at 1 h forecasts while the EnKS-1 is comparable to the EnKS-2 at 48 h forecasts. The "water" in this forecasting system can be divided into three phases: "water" in river routing, which is directly linked to discharge; "water" in catchment routing, which is delayed by the river routing; and "water" in soil moisture, which is further delayed by the catchment routing and influences runoff generation. On one hand, both the EnKS-2 and EnKF-2 update the river routing. Therefore, they exhibit similar forecast abilities at the beginning of the forecasting (Figure 8). However, as the unit hydrograph part is not updated in the EnKF-2 but is updated in the EnKS-2 through the model dynamics using reanalyzed antecedent soil moisture states, the EnKF-2 becomes worse than the

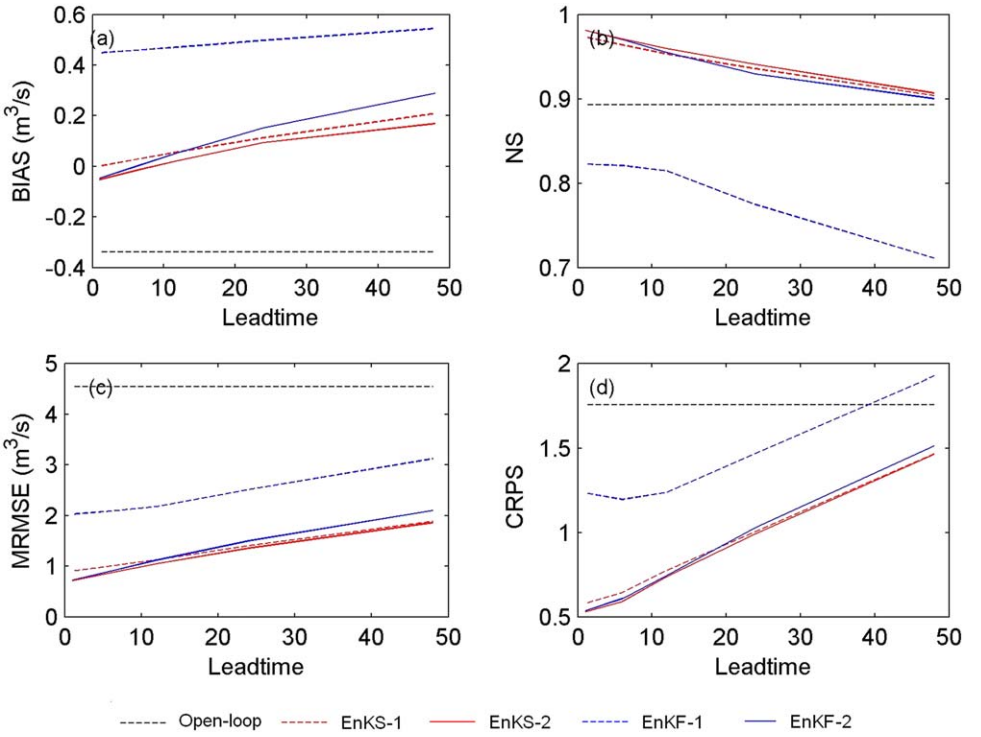

Figure 8. Statistics of forecasts at Myrtleford with the lead time up to 48 h (2005–2010).

EnKS-2 with increasing lead time up to 48 h (Figure 8). On the other hand, both the EnKS-1 and EnKS-2 updated the antecedent states, and that gives equivalent analysis of soil moisture and catchment routing. However, the EnKS-1 does not directly update the river routing, which has more direct effect on shorter term forecasts, thus the EnKS-2 is more accurate than the EnKS-1 for 1 h forecasts (Figure 8). With the increase of the lead time to 48 h, the "water" in catchment routing and soil moisture becomes more important for forecasts, thus the differences between the EnKS-1 and EnKS-2 becomes less significant (Figure 8).

5. Conclusions

In this study, the IEELA scheme is extended to semidistributed hydrologic model updating. A temporally and spatially correlated error structure is estimated through the MAP estimation approach. The lag-aware EnKS is implemented to correct errors in catchment states and river routing states. The results are then compared with the lumped model updating by *Li et al.* [2014] and examined in terms of the "ungauged" internal areas.

The use of the distributed forcing information through a semidistributed model improves open-loop forecasts compared with the lumped model. The improvement from using the semidistributed model becomes less significant after IEELA analysis; however, the small improvement after DA can still be valuable for operational applications. In addition, using distributed systems provides the possibility of obtaining forecasts at ungauged internal sites. While the results in this study show that only one ungauged internal area has a small improvement for short-term forecasts (1–12 h), it is likely that this results from inadequate calibration of the rainfall-runoff model at the subcatchment scale. Most model and error parameters are set to be uniform for all subcatchments in this study. It would be interesting to investigate the impact of using spatially variable parameter sets on the predictability in ungauged areas. Moreover, further improvement in future applications would be expected with improved flow forecasting models, perhaps through incorporation of multiple sources of observations (e.g., remote sensing data). As is widely noted [*Lee et al.*, 2012; *Rakovec et al.*, 2012], there is a trend toward using distributed models for operational hydrologic forecasting, irrespective of consistency with the DA algorithms. Therefore, it is important to keep improving approaches for distributed system updating.

The additional comparison between the EnKS and the EnKF confirms the superiority of the EnKS. From the perspective of state updating, both rainfall-runoff and river routing models should be updated to address all errors in soil-stored water, catchment-routed water, and river-routed water. However, if there is some part of "water" which is not accessible directly by the DA algorithm, the lag-aware DA (e.g., the EnKS) should be implemented to update that part of "water" by using the model dynamics to propagate the updated antecedent states.

Acknowledgments
This work has been financially supported by a CSIRO research studentship and the Water Information Research and Development Alliance betweenthe Australian Bureau of Meteorology and CSIRO. We acknowledge CSIRO Land and Water Flagship, Australian Bureau of Meteorology, and Department of Environment, Land, Water, and Planning, Victoria Government for providing data. We would like to thank Robert Pipunic, Aiswarya Poovakka, three reviewers, and the associate editor for their valuable comments which improve the quality of this paper. Precipitation and potential evapotranspiration data used in this paper can be provided by obtaining permission from CSIRO Land and Water Flagship (QJ.Wang@csiro.au). Streamflow and rating information can be obtained from Department of Environment, Land, Water, and Planning, Victoria Government (http://data.water.vic.gov.au/monitoring.htm). ACCESS precipitation forecasts can be obtained from Australian Bureau of Meteorology (http://www.bom.gov.au/nwp/doc/access/NWPData.shtml).

References

Adams, R., A. W. Western, and A. W. Seed (2012), An analysis of the impact of spatial variability in rainfall on runoff and sediment predictions from a distributed model, *Hydrol. Processes*, *26*(21), 3263–3280, doi:10.1002/hyp.8435.

Ajami, N. K., Q. Duan, and S. Sorooshian (2007), An integrated hydrologic Bayesian multimodel combination framework: Confronting input, parameter, and model structural uncertainty in hydrologic prediction, *Water Resour. Res.*, *43*, W01403, doi:10.1029/2005WR004745.

Alvarez-Garreton, C., D. Ryu, A. W. Western, W. T. Crow, and D. E. Robertson (2014), The impacts of assimilating satellite soil moisture into a rainfall-runoff model in a semi-arid catchment, *J. Hydrol.*, *519*, 2763–2774, doi:10.1016/j.jhydrol.2014.07.041.

Berne, A., G. Delrieu, J.-D. Creutin, and C. Obled (2004), Temporal and spatial resolution of rainfall measurements required for urban hydrology, *J. Hydrol.*, *299*(3–4), 166–179, doi:10.1016/j.jhydrol.2004.08.002.

Candille, G., and O. Talagrand (2005), Evaluation of probabilistic prediction systems for a scalar variable, *Q. J. R. Meteorol. Soc.*, *131*(609), 2131–2150, doi:10.1256/qj.04.71.

Clark, M. P., D. E. Rupp, R. A. Woods, X. Zheng, R. P. Ibbitt, A. G. Slater, J. Schmidt, and M. J. Uddstrom (2008), Hydrological data assimilation with the ensemble Kalman filter: Use of streamflow observations to update states in a distributed hydrological model, *Adv. Water Resour.*, *31*(10), 1309–1324, doi:10.1016/j.advwatres.2008.06.005.

Crow, W. T., and R. H. Reichle (2008), Comparison of adaptive filtering techniques for land surface data assimilation, *Water Resour. Res.*, *44*, W08423, doi:10.1029/2008WR006883.

Crow, W. T., and D. Ryu (2009), A new data assimilation approach for improving runoff prediction using remotely-sensed soil moisture retrievals, *Hydrol. Earth Syst. Sci.*, *13*(1), 1–16, doi:10.5194/hess-13-1-2009.

Crow, W. T., and M. J. van den Berg (2010), An improved approach for estimating observation and model error parameters in soil moisture data assimilation, *Water Resour. Res.*, *46*, W12519, doi:10.1029/2010WR009402.

Crow, W. T., and M. T. Yilmaz (2014), The auto-tuned land data assimilation system (ATLAS), *Water Resour. Res.*, *50*, 371–385, doi:10.1002/2013WR014550.

Crow, W. T., M. J. van den Berg, G. J. Huffman, and T. Pellarin (2011), Correcting rainfall using satellite-based surface soil moisture retrievals: The Soil Moisture Analysis Rainfall Tool (SMART), *Water Resour. Res.*, *47*, W08521, doi:10.1029/2011WR010576.

Cunge, J. A. (1969), On the subject of a flood propagation computation method (Musklngum Method), *J. Hydraul. Res.*, *7*(2), 205–230, doi:10.1080/00221686909500264.

DeChant, C. M., and H. Moradkhani (2011), Radiance data assimilation for operational snow and streamflow forecasting, *Adv. Water Resour.*, *34*(3), 351–364, doi:10.1016/j.advwatres.2010.12.009.

DeChant, C. M., and H. Moradkhani (2012), Examining the effectiveness and robustness of sequential data assimilation methods for quantification of uncertainty in hydrologic forecasting, *Water Resour. Res.*, *48*, W04518, doi:10.1029/2011WR011011.

Duan, Q., S. Sorooshian, and H. V. Gupta (1992), Effective and efficient global optimization for conceptual rainfall-runoff models, *Water Resour. Res.*, *28*(4), 1015–1031, doi:10.1029/91WR02985.

Gupta, H. V., H. Kling, K. K. Yilmaz, and G. F. Martinez (2009), Decomposition of the mean squared error and NSE performance criteria: Implications for improving hydrological modelling, *J. Hydrol.*, *377*(1–2), 80–91, doi:10.1016/j.jhydrol.2009.08.003.

Hamill, T. M. (2001), Interpretation of rank histograms for verifying ensemble forecasts, *Mon. Weather Rev.*, *129*(3), 550–560, doi:10.1175/1520-0493(2001)129<0550:iorhfv>2.0.CO;2.

He, M., T. S. Hogue, S. A. Margulis, and K. J. Franz (2012), An integrated uncertainty and ensemble-based data assimilation approach for improved operational streamflow predictions, *Hydrol. Earth Syst. Sci.*, *16*(3), 815–831, doi:10.5194/hess-16–815-2012.

Hendricks Franssen, H. J., and W. Kinzelbach (2008), Real-time groundwater flow modeling with the Ensemble Kalman Filter: Joint estimation of states and parameters and the filter inbreeding problem, *Water Resour. Res.*, *44*, W09408, doi:10.1029/2007WR006505.

Kavetski, D., G. Kuczera, and S. W. Franks (2006), Bayesian analysis of input uncertainty in hydrological modeling: 1. Theory, *Water Resour. Res.*, *42*, W03407, doi:10.1029/2005WR004368.

Khakbaz, B., B. Imam, K. Hsu, and S. Sorooshian (2012), From lumped to distributed via semi-distributed: Calibration strategies for semi-distributed hydrologic models, *J. Hydro.*, *418-419*, 61–77, doi:10.1016/j.jhydrol.2009.02.021.

Komma, J., G. Bloschl, and C. Reszler (2008), Soil moisture updating by ensemble Kalman filtering in real-time flood forecasting, *J. Hydrol.*, *357*(3–4), 228–242, doi:10.1016/j.jhydrol.2008.05.020.

Krajewski, W. F. (1987), Cokriging radar-rainfall and rain gage data, *J. Geophys. Res.*, *92*(D8), 9571–9580, doi:10.1029/JD092iD08p09571.

Lee, H., D.-J. Seo, and V. Koren (2011), Assimilation of streamflow and in situ soil moisture data into operational distributed hydrologic models: Effects of uncertainties in the data and initial model soil moisture states, *Adv. Water Resour.*, *34*(12), 1597–1615, doi:10.1016/j.advwatres.2011.08.012.

Lee, H., D.-J.Seo, Y. Liu, V. Koren, P. McKee, and R. Corby (2012), Variational assimilation of streamflow into operational distributed hydrologic models: Effect of spatiotemporal scale of adjustment, *Hydrol. Earth Syst. Sci.*, *16*(7), 2233–2251, doi:10.5194/hess-16–2233-2012.

Leisenring, M., and H. Moradkhani (2012), Analyzing the uncertainty of suspended sediment load prediction using sequential data assimilation, *J. Hydrol.*, *468–469*, 268–282, doi:10.1016/j.jhydrol.2012.08.049.

Li, Y., D. Ryu, Q. J. Wang, T. C. Pagano, W. A. Western, P. Hapuarachchi, and P. Toscas (2011), Assimilation of streamflow discharge into a continuous flood forecasting model, in *Proceedings of Symposium H03 Held During IUGG GA 2011 in Melbourne*, edited by G. Blöschl et al., pp. 107–113, IAHS Publ., Melbourne, Australia.

Li, Y., D. Ryu, A. W. Western, and Q. J. Wang (2013), Assimilation of stream discharge for flood forecasting: The benefits of accounting for routing time lags, *Water Resour. Res.*, *49*, 1887–1900, doi:10.1002/wrcr.20169.

Li, Y., D. Ryu, A. W. Western, Q. J. Wang, D. E. Robertson, and W. T. Crow (2014), An integrated error parameter estimation and lag-aware data assimilation scheme for real-time flood forecasting, *J. Hydrol.*, *519*, 2722–2736, doi:10.1016/j.jhydrol.2014.08.009.

Liu, Y. Q., et al. (2012), Advancing data assimilation in operational hydrologic forecasting: Progresses, challenges, and emerging opportunities, *Hydrol. Earth Syst. Sci.*, *16*(10), 3863–3887, doi:10.5194/hess-16–3863-2012.

Lü, H., T. Hou, R. Horton, Y. Zhu, X. Chen, Y. Jia, W. Wang, and X. Fu (2013), The streamflow estimation using the Xinanjiang rainfall runoff model and dual state-parameter estimation method, *J. Hydrol.*, *480*, 102–114, doi:10.1016/j.jhydrol.2012.12.011.

Massari, C., L. Brocca, S. Barbetta, C. Papathanasiou, M. Mimikou, and T. Moramarco (2014), Using globally available soil moisture indicators for flood modelling in Mediterranean catchments, *Hydrol. Earth Syst. Sci.*, *18*(2), 839–853, doi:10.5194/hess-18–839-2014.

McMillan, H. K., B. Jackson, M. Clark, D. Kavetski, and R. Woods (2011), Rainfall uncertainty in hydrological modelling: An evaluation of multiplicative error models, *J. Hydrol.*, *400*(1–2), 83–94, doi:10.1016/j.jhydrol.2011.01.026.

McMillan, H. K., E. Ö. Hreinsson, M. P. Clark, S. K. Singh, C. Zammit, and M. J. Uddstrom (2013), Operational hydrological data assimilation with the recursive ensemble Kalman filter, *Hydrol. Earth Syst. Sci.*, *17*(1), 21–38, doi:10.5194/hess-17–21-2013.

Misirli, F., H. V. Gupta, and S. Sorooshian (2002), Bayesian recursive estimation of parameter and output uncertainty for watershed models, in *AGU Monograph: Advances in Model Calibration*, edited by Q. Duan et al., AGU, Washington, D. C.

Moradkhani, H., C. M. DeChant, and S. Sorooshian (2012), Evolution of ensemble data assimilation for uncertainty quantification using the particle filter-Markov chain Monte Carlo method, *Water Resour. Res.*, *48*, W02501, doi:10.1029/2012WR012144.

Nash, J. E. (1959), A note on the Muskingum flood-routing method, *J. Geophys. Res.*, *64*(8), 1053–1056, doi:10.1029/JZ064i008p01053.

Nash, J. E., and J. V. Sutcliffe (1970), River flow forecasting through conceptual models part I: A discussion of principles, *J. Hydrol.*, *10*(3), 282–290, doi:10.1016/0022–1694(70)90255-6.

Nie, S., J. Zhu, and Y. Luo (2011), Simultaneous estimation of land surface scheme states and parameters using the ensemble Kalman filter: Identical twin experiments, *Hydrol. Earth Syst. Sci.*, *15*(8), 2437–2457, doi:10.5194/hess-15–2437-2011.

Nijssen, B., and D. P. Lettenmaier (2004), Effect of precipitation sampling error on simulated hydrological fluxes and states: Anticipating the Global Precipitation Measurement satellites, *J. Geophys. Res.*, *109*, D02103, doi:10.1029/2003JD003497.

Noh, S. J., Y. Tachikawa, M. Shiiba, and S. Kim (2011), Applying sequential Monte Carlo methods into a distributed hydrologic model: Lagged particle filtering approach with regularization, *Hydrol. Earth Syst. Sci.*, *15*(10), 3237–3251, doi:10.5194/hess-15–3237-2011.

Pagano, T. C., P. Hapuarachchi, and Q. J. Wang (2010), Continuous rainfall-runoff model comparison and short-term daily streamflow forecast skill evaluation, CSIRO technical report EP103545, 70 pp. CSIRO Water for a Healthy Country National Research Flagship, CSIRO Land and Water.

Pagano, T. C., Q. J. Wang, P. Hapuarachchi, and D. Robertson (2011a), A dual-pass error-correction technique for forecasting streamflow, *J. Hydrol.*, *405*(3–4), 367–381, doi:10.1016/j.jhydrol.2011.05.036.

Pagano, T. C., P. Ward, X. N. Wang, P. Hapuarachchi, D. L. Shrestha, J. Anticev, and Q. J. Wang (2011b), The SWIFT calibration cookbook: Experience from the Ovens, CSIRO technical report, 78 pp., CSIRO: Water for a Healthy Country Natl. Res. Flagship, Highett, Victoria, Australia.

Pauwels, V. R. N., and G. J. M. De Lannoy (2009), Ensemble-based assimilation of discharge into rainfall-runoff models: A comparison of approaches to mapping observational information to state space, *Water Resour. Res.*, *45*, W08428, doi:10.1029/2008WR007590.

Rakovec, O., A. H. Weerts, P. Hazenberg, P. J. J. F. Torfs, and R. Uijlenhoet (2012), State updating of a distributed hydrological model with Ensemble Kalman Filtering: Effects of updating frequency and observation network density on forecast accuracy, *Hydrol. Earth Syst. Sci.*, *16*(9), 3435–3449, doi:10.5194/hess-16–3435-2012.

Raupach, M. R., P. R. Briggs, V. Haverd, E. A. King, M. Paget, and C. M. Trudinger (2009), Australian Water Availability Project (AWAP): CSIRO Marine and Atmospheric Research Component: Final Report for Phase 3, CAWCR technical report 13, 67 pp., Centre for Australian Weather and Climate Research, Melbourne, Victoria, Australia.

Raupach, M. R., P. R. Briggs, V. Haverd, E. A. King, M. Paget, and C. M. Trudinger (2012), *Australian Water Availability Project* CSIRO Mar. and Atmos. Res., Australia.

Reichle, R. H., W. T. Crow, and C. L. Keppenne (2008), An adaptive ensemble Kalman filter for soil moisture data assimilation, *Water Resour. Res.*, *44*, W03423, doi:10.1029/2007WR006357.

Renard, B., D. Kavetski, E. Leblois, M. Thyer, G. Kuczera, and S. W. Franks (2011), Toward a reliable decomposition of predictive uncertainty in hydrological modeling: Characterizing rainfall errors using conditional simulation, *Water Resour. Res.*, *47*, W11516, doi:10.1029/2011WR010643.

Ricci, S., A. Piacentini, O. Thual, E. Le Pape, and G. Jonville (2011), Correction of upstream flow and hydraulic state with data assimilation in the context of flood forecasting, *Hydrol. Earth Syst. Sci.*, *15*(11), 3555–3575, doi:10.5194/hess-15–3555-2011.

Salamon, P., and L. Feyen (2009), Assessing parameter, precipitation, and predictive uncertainty in a distributed hydrological model using sequential data assimilation with the particle filter, *J. Hydrol.*, *376*(3–4), 428–442, doi:10.1016/j.jhydrol.2009.07.051.

Seed, A. W., R. Srikanthan, and M. Menabde (1999), A space and time model for design storm rainfall, *J. Geophys. Res.*, *104*(D24), 31,623–31,630, doi:10.1029/1999jd900767.

Seed, A. W., C. Draper, R. Srikanthan, and M. Menabde (2000), A multiplicative broken-line model for time series of mean areal rainfall, *Water Resour. Res.*, *36*(8), 2395–2399, doi:10.1029/2000WR900117.

Seed, A. W., R. Srikanthan, and B. F. Taylor (2002), Stochastic space-time rainfall for designing urban drainage systems, paper presented at International Conference on Urban Hydrology for the 21st Century, Kuala Lumpur, Malaysia, 14–16 Oct.

Seo, D.-J., L. Cajina, R. Corby, and T. Howieson (2009), Automatic state updating for operational streamflow forecasting via variational data assimilation, *J. Hydrol.*, *367*(3–4), 255–275, doi:10.1016/j.jhydrol.2009.01.019.

Smith, J. A., and W. F. Krajewski (1991), Estimation of the mean field bias of radar rainfall estimates, *J. Appl. Meteorol.*, *30*(4), 397–412, doi:10.1175/1520-0450(1991)030<0397:EOTMFB>2.0.CO;2.

Sorenson, H. W. (1980), *Parameter Estimation: Principles and Problems*, 398 pp., Marcel Dekker, New York.

Sun, X., R. G. Mein, T. D. Keenan, and J. F. Elliott (2000), Flood estimation using radar and rain gauge data, *J. Hydrol.*, *239*(1–4), 4–18, doi:10.1016/S0022–1694(00)00350-4.

Thirel, G., E. Martin, J. F. Mahfouf, S. Massart, S. Ricci, and F. Habets (2010a), A past discharges assimilation system for ensemble streamflow forecasts over France: Part 1: Description and validation of the assimilation system, *Hydrol. Earth Syst. Sci.*, *14*(8), 1623–1637, doi:10.5194/hess-14–1623-2010.

Thirel, G., E. Martin, J.-F.Mahfouf, S. Massart, S. Ricci, F. Regimbeau, and F. Habets (2010b), A past discharge assimilation system for ensemble streamflow forecasts over France: Part 2: Impact on the ensemble streamflow forecasts, *Hydrol. Earth Syst. Sci.*, *14*(8), 1639–1653, doi:10.5194/hess-14–1639-2010.

Velasco-Forero, C. A., D. Sempere-Torres, E. F. Cassiraga, and J. Jaime Gómez-Hernández (2009), A non-parametric automatic blending methodology to estimate rainfall fields from rain gauge and radar data, *Adv. Water Resour.*, *32*(7), 986–1002, doi:10.1016/j.advwatres.2008.10.004.

Vrugt, J. A., H. V. Gupta, and B. O. Nuallain (2006), Real-time data assimilation for operational ensemble streamflow forecasting, *J. Hydrometeorol.*, *7*(3), 548–565, doi:10.1175/JHM504.1.

Vrugt, J. A., C. J. F. terBraak, M. P. Clark, J. M. Hyman, and B. A. Robinson (2008), Treatment of input uncertainty in hydrologic modeling: Doing hydrology backward with Markov chain Monte Carlo simulation, *Water Resour. Res.*, *44*, W00B09, doi:10.1029/2007WR006720.

Vrugt, J. A., C. J. F. terBraak, C. G. H. Diks, and G. Schoups (2013), Hydrologic data assimilation using particle Markov chain Monte Carlo simulation: Theory, concepts and applications, *Adv. Water Resour.*, *51*, 457–478, doi:10.1016/j.advwatres.2012.04.002.

Wanders, N., D. Karssenberg, A. de Roo, S. M. de Jong, and M. F. P. Bierkens (2014), The suitability of remotely sensed soil moisture for improving operational flood forecasting, *Hydrol. Earth Syst. Sci.*, *18*(6), 2343–2357, doi:10.5194/hess-18–2343-2014.

Wang, D., Y. Chen, and X. Cai (2009), State and parameter estimation of hydrologic models using the constrained ensemble Kalman filter, *Water Resour. Res.*, *45*, W11416, doi:10.1029/2008WR007401.

Weerts, A. H., and G. Y. H. El Serafy (2006), Particle filtering and ensemble Kalman filtering for state updating with hydrological conceptual rainfall-runoff models, *Water Resour. Res.*, *42*, W09403, doi:10.1029/2005WR004093.

Xie, X. H., and D. X. Zhang (2010), Data assimilation for distributed hydrological catchment modeling via ensemble Kalman filter, *Adv. Water Resour.*, *33*(6), 678–690, doi:10.1016/j.advwatres.2010.03.012.

Zhang, Y., F. H. S. Chiew, L. Zhang, and H. Li (2009), Use of remotely sensed actual evapotranspiration to improve rainfall–runoff modeling in southeast Australia, *J. Hydrometeorol.*, *10*(4), 969–980, doi:10.1175/2009JHM1061.1.